Hindawi
Advances in Civil Engineering
Volume 2020, Article ID 8858363, 13 pages
https://doi.org/10.1155/2020/8858363

Research Article

Triaxial Strength Criteria in Mohr Stress Space for Intact Rocks

Baohua Guo,[1,2,3] **Long Wang**,[4] **Yizhe Li**,[1] **and Yan Chen**[1]

[1]*School of Energy Science and Engineering, Henan Polytechnic University, Jiaozuo 454000, China*
[2]*Collaborative Innovation Center of Coal Work Safety, Jiaozuo 454000, China*
[3]*Key Laboratory of Safety and High-efficiency Coal Mining, Ministry of Education (Anhui University of Science and Technology), Huainan 232001, China*
[4]*College of Safety Science and Engineering, Henan Polytechnic University, Jiaozuo 454003, China*

Correspondence should be addressed to Long Wang; 18336860596@163.com

Received 11 June 2020; Revised 15 September 2020; Accepted 1 October 2020; Published 20 October 2020

Academic Editor: Fengqiang Gong

Conventional triaxial strength criteria are important for the judgment of rock failure. Linear, parabolic, power, logarithmic, hyperbolic, and exponential equations were, respectively, established to fit the conventional triaxial compression test data for 19 types of rock specimens in the Mohr stress space. Then, a method for fitting the failure envelope to all common tangent points of each two adjacent Mohr's circles (abbreviated as CTPAC) was proposed in the Mohr stress space. The regression accuracy of the linear equation is not as good as those of the nonlinear equations on the whole, and the regression uniaxial compression strength $(\sigma_c)_r$, tensile strength $(\sigma_t)_r$, cohesion c_r, and internal frictional angle φ_r predicted by the regression linear failure envelopes with the method for fitting the CTPAC in the Mohr stress space are close to those predicted in the principal stress space. Therefore, the method for fitting CTPAC is feasible to determine the failure envelopes in the Mohr stress space. The logarithmic, hyperbolic, and exponential equations are recommended to obtain the failure envelope in the Mohr stress space when the data of tensile strength $(\sigma_t)_t$ are or are not included in regression owing to their higher R^2, less positive x-intercepts, and more accurate regression cohesion c_r. Furthermore, based on the shape and development trend of the nonlinear strength envelope, it is considered that when the normal stress is infinite, the total bearing capacity of rock tends to be a constant after gradual increase with decreasing rates. Thus, the hyperbolic equation and the exponential equation are more suitable to fit triaxial compression strength in a higher maximum confining pressure range because they have limit values. The conclusions can provide references for the selection of the triaxial strength criterion in practical geotechnical engineering.

1. Introduction

The Mohr-Coulomb strength criterion has been widely applied in rock engineering. Cohesion c and internal friction angle φ obtained from the conventional triaxial compression tests are commonly used as strength parameters of rock. Rock is a kind of anisotropic material with natural fractures and defects, and inaccuracies, such as loading cell friction, end plate roughness, and membrane stiffness, are inevitable in the triaxial compression tests, so it is hard for Mohr-Coulomb failure envelope to be tangent to all Mohr's circles [1–4]. Many scholars put forward various methods to obtain more accurate strength parameters of rock. Stafford et al. [4] suggested a method of resorting to a plot of $(\sigma_1-\sigma_3)/2$ against $(\sigma_1+\sigma_3)/2$ for each test and drawing the best fitting straight line through the points and then deriving c and φ from this as shown in Figure 1(a). Another common method is to use a linear equation to fit the relationship between the major principal stress σ_1 and the minor principal stress σ_3 at failure with the least square method as shown in Figure 1(b), and then 6~8 points are equidistantly selected on the regression line to determine Mohr's circles. Finally, the linear regression failure envelope can be drawn based on the common tangent points of all Mohr's circles, and thus c and φ can be obtained as shown in Figure 1(c). Yang et al. [6] presented a linear equation obtained by fitting the relationship between σ_1 and σ_3 with the least square method, in which the slope and the y-intercept of the regression line are obtained, and c

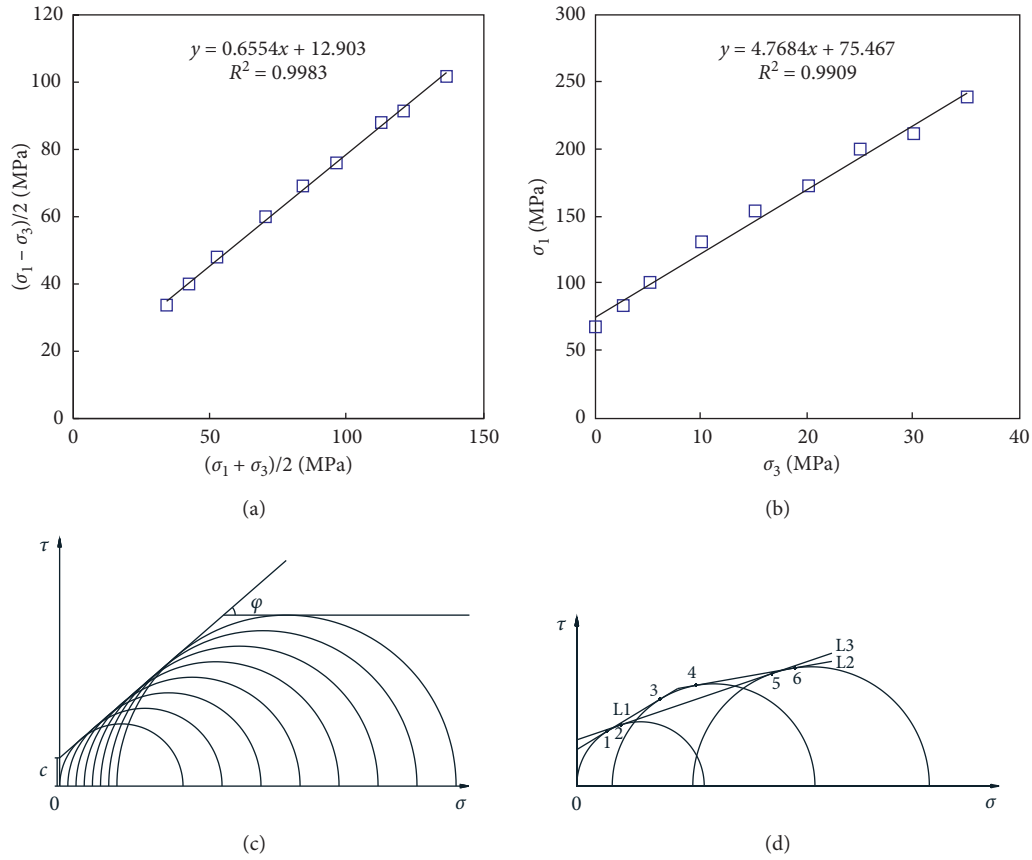

Figure 1: Methods of obtaining strength criteria. (a) The method by Stafford et al. [4]. (b) A linear curve in the common method. (c) Mohr's circles in the common method. (d) The method by Wang [5].

and φ can be further calculated. Wang firstly calculated the coordinates of common tangent points on each two Mohr's circles, and then c and φ can be predicted by fitting a straight line to all the common tangent points with the least square method [5]. For example, in Figure 1(d), there are three Mohr circles, three common tangent lines, and six common tangent points, which are used to obtain the linear regression failure envelope.

With the increasing depth in geotechnical engineering, the rock failure mechanism changes, and the brittle rock under a low confining pressure gradually presents ductile failure feature under a higher confining pressure [7]. Moreover, the differential stress (σ_1–σ_3) at failure of rock would approach being a constant, and the dip angle of the failure plane is close to $\pi/4$ when the maximum confining pressure becomes high enough [8]. In this case, the inaccuracy is quite large using a linear equation to obtain the failure envelope, so that the above-mentioned methods of determining linear strength envelopes are unavailable. Therefore, the nonlinear equations are needed to fit the test data. Specifically, when using Wang's method to get c and φ, the slope of common tangent line is relatively steep for two adjacent Mohr's circles under low confining pressures, and then it gradually tends to be gentle with the increase in confining pressure. Theoretically, for two nonadjacent Mohr's circles, the farther the distance between them, the smaller the slope of common tangent line. Moreover, the common tangent points will significantly differ from those on the adjacent Mohr's circles, which may result in an unavailable failure envelope. Thus, the common tangent points on only two adjacent Mohr's circles (CTPAC) are adopted here to obtain the failure envelope. In particular, we use only four common tangent points 1, 3, 4, and 6 generated from the two common tangent lines L1 and L2 and three Mohr's circles to obtain the rock failure envelope as shown in Figure 1(d).

As mentioned above, the nonlinear strength envelope can obtain a better fitting accuracy and reflects the bearing characteristics of rock more accurately in a larger range of the maximum confining pressure. Many studies have been conducted on the nonlinear strength criteria [8–13], in which You compared 16 strength criteria composed of one, two, and three parameters, respectively. In this paper, some empirical equations for conventional triaxial strength criteria of intact rock are proposed and studied comparatively. From the review authored by Cartrin [14], most empirical formulas of strength criteria are simple elementary function forms, such as power function, exponential function, and logarithmic function, and most of them are in the form of power function. Among them, linear function, parabolic function, and hyperbolic function can be regarded as the variation form of power function. Therefore, this paper

mainly focuses on the applicability of linear equation, parabolic equation, power equation, logarithmic equation, hyperbolic equation, and exponential equation in describing the intact rock strength criterion. Finally, more suitable empirical equations are recommended based on the bearing mechanism of rock.

2. Conventional Triaxial Strengths and Empirical Equations

2.1. Test Data of Conventional Triaxial Strengths. Table 1 shows σ_1 and σ_3 at failure of red sandstone (RS) [15], Tyndall limestone (TL) [16], Lac du Bonnet granite (LG) [16], Dunham dolomite (DD) [17], Inada granite (IG) [17], Mizuho trachyte (MT) [17], Marazuru andesite (MA) [17], Orikable monzonite (OM) [17], Bunt sandstone (BS) [18], Yamaguchi marble (YM) [18], Solnhofen limestone (SL) [18], Carrara marble (CM) [18], Granite (G) [19], Quartzite (Q) [19], and Basalt (B) [19]. Moreover, σ_1 and σ_3 at failure of powder-grained marble (PGM), fine-grained marble (FGM), middle-grained marble (MGM), and coarse-grained marble (CGM) were obtained using RMT-150B rock mechanics test machine and are also shown in Table 1.

When the test data of uniaxial tensile strength $(\sigma_t)_t$ and uniaxial compressive strength $(\sigma_c)_t$ are included in the parameters calculation of the Hoek-Brown strength criterion, a better fitting result than that using only the triaxial data can be obtained [9]. Therefore, whether the tensile strength data $(\sigma_t)_t$ should be included in regression is discussed here, and the tensile strengths of seven kinds of rock are listed in Table 1.

The marble samples were collected from a quarry in Nanyang City, Henan Province, and the main minerals are calcite, dolomite, and magnesite. According to the requirements of the International Society of Rock Mechanics (ISRM), the standard cylindrical specimens with the diameter of 50 mm and the length of 100 mm were prepared, as shown in Figure 2(a).

After treating *P* wave testing on rock specimens with the ultrasonic detector (Figure 2(b)), a serious test of uniaxial compression, Brazilian splitting and triaxial compression were conducted using the RMT-150B electrohydraulic servo rock mechanics testing system developed by Wuhan Institute of Geotechnical Engineering, Chinese Academy of Sciences (Figure 2(c)). The basic mechanical parameters of rock, such as uniaxial compressive strength, tensile strength, internal friction angle, cohesion, elastic modulus, and Poisson's ratio, were obtained, as shown in Table 2. The axial and lateral loading capacities of this system are 100 t and 50 t, respectively. One vertical displacement sensor with the stroke of 20 mm was used to monitor the axial deformation of rock specimen, and two horizontal displacement sensors with the stroke of 2.5 mm were used to monitor the transverse deformation of rock specimen.

2.2. Empirical Equations. Six equations (linear, parabola, power, logarithm, hyperbola, and exponent) were used here to fit the failure curves, respectively, in the Mohr stress space. When the conventional strength criteria are fitted to CTPAC in the Mohr stress space, it should be ensured that each two adjacent Mohr's circles cannot wrap each other, because their common tangent points are not obtained. Besides, the latter Mohr's circle (the center is located on the right side) should be removed in regression if its diameter is smaller than that of a former one (the center is located on the left side), because it is unreasonable that the common tangent points locate on the right side of the vertex of a Mohr's circle. The removed data in specimens MA, SL, Q, B, and PGM were marked with $*$ as shown in Table 1.

The linear equation is

$$\tau = a_1\sigma + b_1, \tag{1}$$

where a_1 and b_1 are the regression.

The parabolic equation is

$$\tau = \sqrt{a_2(\sigma - b_2)}, \tag{2}$$

where a_2 and b_2 are the regression constants and $a_2 > 0$, $x > -b_2$, and $\sigma > b_2$.

The power equation is

$$\tau = \left(\frac{\sigma - d_3}{a_3}\right)^{1/b_3}, \tag{3}$$

where a_3, b_3, and d_3 are regression constants and $a_3 > 0$, $b_3 > 1$, and $\sigma > d_3$.

The logarithmic equation is

$$\tau = a_4 \ln(\sigma + b_4) + d_4, \tag{4}$$

where a_4, b_4, and d_4 are regression constants and $a_4 > 0$.

The hyperbolic equation is

$$\tau = \frac{1}{a_5}\left(\frac{1}{\sigma - d_5} + \frac{1}{a_5 b_5}\right)^{-1}, \tag{5}$$

where a_5, b_5, and d_3 are regression constants and $a_3 > 0$ and $\sigma > d_3$. The slope of regression failure envelope k, $k_5 = a_5^3 b_5^2/(x + a_5 b_5 d_5)^2$, decreases with increasing σ. When $\sigma = \infty$, $k = 0$, and $\tau = b_5$, the radius of the ultimate Mohr's circle in Mohr stress space b_3 does not increase with σ.

The exponential equation is

$$\tau = a_6\left(1 - e^{-\sigma/b_6}\right) + d_6, \tag{6}$$

where a_6, b_6, and d_6 are regression constants, and $a_6 > 0$ and $b_6 > 0$. In the Mohr stress space, the slope of regression failure envelope k decreases with increasing σ. When $\sigma = \infty$, $k = 0$, $\tau = a_6 + d_6$, and $y = a_6 + d_6$, the radius of the ultimate Mohr's circle in the Mohr stress space does not increase with σ_3.

3. Regression Results of Linear Strength Criterion

In this paper, the newly added subscript t expresses the test values, the subscript r expresses the regression values, the subscript m expresses the values in the Mohr stress space, and the subscript p expresses the values in the principal

Table 1: Conventional triaxial compression strengths (MPa).

Rock		σ_3 and σ_1 at failure														
RS [15]	σ_3	−3.46	0	2.5	5	10	15	20	25	30	35					
	σ_1	0	68	83.1	100.9	130.3	153.4	172.3	200.3	212.1	238.3					
TL [16]	σ_3	−3.8	0	5	10	15	20	25	30	35	40					
	σ_1	0	52	88	106	118	137	149	164	176	190					
LG [16]	σ_3	−13	0	4	5	7	10	12	14	18	21	25	30	35	40	
	σ_1	0	226	289	317	337	365	396	426	445	487	528	571	593	637	
DD [17]	σ_3		0	25	45	60	65	85	105	125						
	σ_1		262	400	487	540	568	620	682	725						
IG [17]	σ_3		0	20	40	70	100	150	200	230						
	σ_1		229	508	692	860	1013	1168	1374	1497						
MT [17]	σ_3		0	15	30	45	60	75	100							
	σ_1		100	196	259	302	341	368	437							
MA [17]	σ_3		0	16	20	40	70	100	110	130*						
	σ_1		140	349	372.5	552	671	806	875	881						
OM [17]	σ_3		0	5	20	40	80	140	200							
	σ_1		234	339	504	584.7	751.3	962	1107							
BS [18]	σ_3		0	6	12.5	25	40	55	70	85	100	150	200			
	σ_1		81	113	130	175	210	246	272	295	324	397	454			
YM [18]	σ_3		0	5	10	20	30	40	50	60	70	80	90	100		
	σ_1		60	100	122	154	193	221	253	275	310	323	346	361		
SL [18]	σ_3		0	6	15	24	46	72	111	162	195*	304*				
	σ_1		293	335	360	381	426	467	518	558	595	709				
CM [18]	σ_3		0	25	50	68.4	85.5									
	σ_1		137	234	314	358	404									
G [19]	σ_3		0	32	100	120	150	200	300	400	500	600				
	σ_1		233	630	1030	1180	1310	1380	1670	2135	2320	2650				
Q [19]	σ_3		0	100	300	400*	500									
	σ_1		327	1297.5	2430	2480	2986									
B [19]	σ_3		0	150	200	300*	400	500	550	600*						
	σ_1		349	1455	1400	1490	1860	2020	2320	2340						
PGM	σ_3	−1.78	0	5	10	15	20	25*								
	σ_1	0	141.68	176.86	192.2	204.31	221.7	225.8								
FGM	σ_3	−2.826	0	5	10	15	20	25								
	σ_1	0	70.93	95.52	107.9	118.34	133.3	146.3								
MGM	σ_3	−2.137	0	5	10	15	20	25								
	σ_1	0	65.17	94.33	119.4	131.81	143	152.4								
CGM	σ_3	−1.568	0	5	10	15	20	25								
	σ_1	0	48.38	72.3	90.03	96.52	113.2	122.5								

*Removed when fitting a strength envelope in the Mohr stress space.

Figure 2: Specimen and test equipment: (a) marble specimen; (b) ultrasonic detector; (c) RMT-150B rock mechanical test system.

Table 2: Summary of mechanical parameters of marble specimens.

Group	Particle size (mm)	Color	UCS (MPa)	Elastic modulus (GPa)	Poisson's ratio	Frictional angle (°)	Cohesion (MPa)	P wave (m/s)
PGM	0.2~0.5	Grey	141.68	83.87	0.377	25.28	50.90	5854.56
FGM	0.5~1	Pink	70.93	47.45	0.316	25.28	25.79	5235.98
MGM	1~3	Pink	65.17	53.12	0.293	23.6	28.96	5270.34
CGM	3~5	White	48.38	41.88	0.119	30.0	15.04	5414.74

stress space. Moreover, the subscript u means that $(\sigma_t)_t$ is not included in regression, while the subscript i means that $(\sigma_t)_t$ is included in regression. For example, $(\sigma_t)_t$ means a test tensile strength value of a rock specimen, and $(\sigma_c)_{\mathrm{rmu}}$ means a regression compressive strength value of a rock specimen obtained in the Mohr stress space with $(\sigma_t)_t$ not being included in regression.

The linear strength criterion is most commonly used in geotechnical engineering. Thus, it is necessary to analyze the following contents, including the regression results of the linear equation in the Mohr stress space and in the principal stress space, the influences of $(\sigma_t)_t$ contained in regression on the validity of regression, and the applicability of fitting strength envelopes to CTPAC in the Mohr stress space.

3.1. Regression Squared Correlation Coefficient. Figure 3 shows the regression squared correlation coefficients R^2 of linear equation in two different stress spaces. With $(\sigma_t)_t$ being included in regression in the principal stress space, the minimum (0.632), the average (0.844), and the maximum (0.958) of $(R^2)_{\mathrm{rpi}}$ of linear equation are all lowest. The regression coefficients $(R^2)_{\mathrm{rmi}}$ of linear equation in the Mohr stress space with $(\sigma_t)_t$ included in regression were shown as follows, with the minimum, average, and maximum values of 0.923, 0.948, and 0.983, respectively. However, when $(\sigma_t)_t$ is not included in regression, the average R^2 are all above 0.961 and the maximum R^2 are all above 0.991. Thus, R^2 of linear equation would generally reduce when $(\sigma_t)_t$ is included in the regression.

3.2. Regression Strength Parameters. The strength parameters of rock (c, φ) are usually determined by fitting a line to common tangent points on the ultimate Mohr's circles in the Mohr stress space, and then $(\sigma_c)_r$ and $(\sigma_t)_r$ can be calculated from the regression line (linear Mohr-Coulomb criterion) in application. Especially in this paper, the linear strength envelopes were fitted to CTPAC in the Mohr stress space. Besides, $(\sigma_c)_r$, $(\sigma_t)_r$, c_r, and φ_r also can be predicted by fitting the relationship between σ_1 and σ_3 at failure in principal stress space using equation (1). If $(\sigma_c)_r$, $(\sigma_t)_r$, c_r, and φ_r predicted by above two methods have no obvious differences, the linear strength envelope fitted to CTPAC can be considered in the application.

Figure 4 shows $(\sigma_c)_r$, Abs. $(\sigma_t)_r$, c_r, and φ_r predicted by above two methods. In Figure 4(a), $(\sigma_c)_{\mathrm{rpu}}$ has a linear relation with $(\sigma_c)_{\mathrm{rmu}}$ and they are almost equivalent with each other. $(\sigma_c)_{\mathrm{rpi}}$ and $(\sigma_c)_{\mathrm{rmi}}$ are also equivalent with each other, and they are both lower than the corresponding $(\sigma_c)_{\mathrm{rpu}}$ and $(\sigma_c)_{\mathrm{rmu}}$. However $(\sigma_c)_{\mathrm{rpi}}$ and $(\sigma_c)_{\mathrm{rmi}}$ are closer to $(\sigma_c)_t$ than

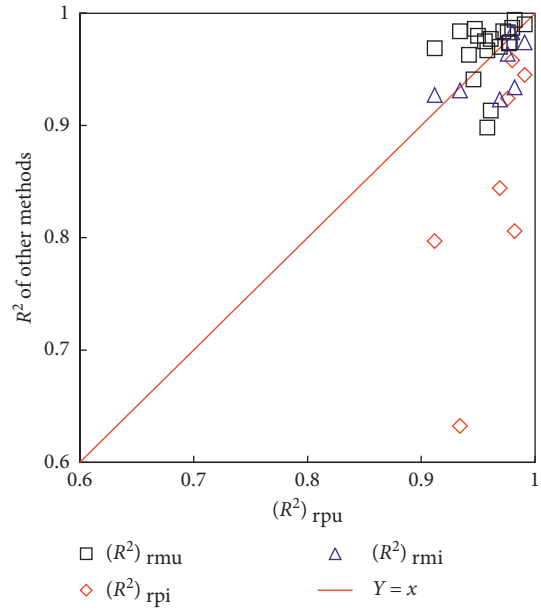

Figure 3: Regression squared correlation coefficient of equation (1) in two stress spaces.

$(\sigma_c)_{\mathrm{rpu}}$ and $(\sigma_c)_{\mathrm{rmu}}$. $(\sigma_c)_t$ is lower than $(\sigma_c)_{\mathrm{rpu}}$, and it has an exponential relation with $(\sigma_c)_{\mathrm{rpu}}$, which is expressed as follows:

$$\sigma_{\mathrm{ct}} = 382.08 \times \left(1 - \exp\left(\frac{-\sigma_{\mathrm{crpu}}}{274.76}\right)\right) - 32.35, \quad (7)$$

in which R^2 is 0.894. Therefore, equation (7) can be used to modify $(\sigma_c)_{\mathrm{rpu}}$ for more accurate estimation of the value of $(\sigma_c)_t$.

In Figure 4(b), Abs. $(\sigma_t)_{\mathrm{rpu}}$ is about equal to Abs. $(\sigma_t)_{\mathrm{rmu}}$, and it has a linear relation with Abs. $(\sigma_t)_{\mathrm{rmu}}$, but there is some difference between them in a higher part of Abs. $(\sigma_t)_{\mathrm{rmu}}$. Abs. $(\sigma_t)_{\mathrm{rpi}}$ and Abs. $(\sigma_t)_{\mathrm{rmi}}$ are close to each other, and they are both lower than the corresponding Abs. $(\sigma_t)_{\mathrm{rpu}}$ and Abs. $(\sigma_t)_{\mathrm{rmu}}$ but higher than Abs. $(\sigma_t)_t$. The difference between Abs. $(\sigma_t)_{\mathrm{rpi}}$, Abs. $(\sigma_t)_{\mathrm{rmi}}$, and Abs. $(\sigma_t)_t$ would also increase with increasing Abs. $(\sigma_t)_{\mathrm{rmu}}$ on the whole. Thus, it is recommended to get more accurate $(\sigma_t)_r$ using $(\sigma_t)_t$ in regression.

Similarly, in Figure 4(c), when $(\sigma_t)_t$ is not included in regression, c_{rpu} is about equal to c_{rmu}, and it has a linear relation with c_{rmu}. However, there is some difference between them in the higher part of c_{rmu}. When $(\sigma_t)_t$ is included in regression, c_{rpi} and c_{rmi} are close to each other, and they are both lower than the corresponding c_{rpu} and c_{rmu}. In Figure 4(d), when $(\sigma_t)_t$ is not included in regression, φ_{rpu} is

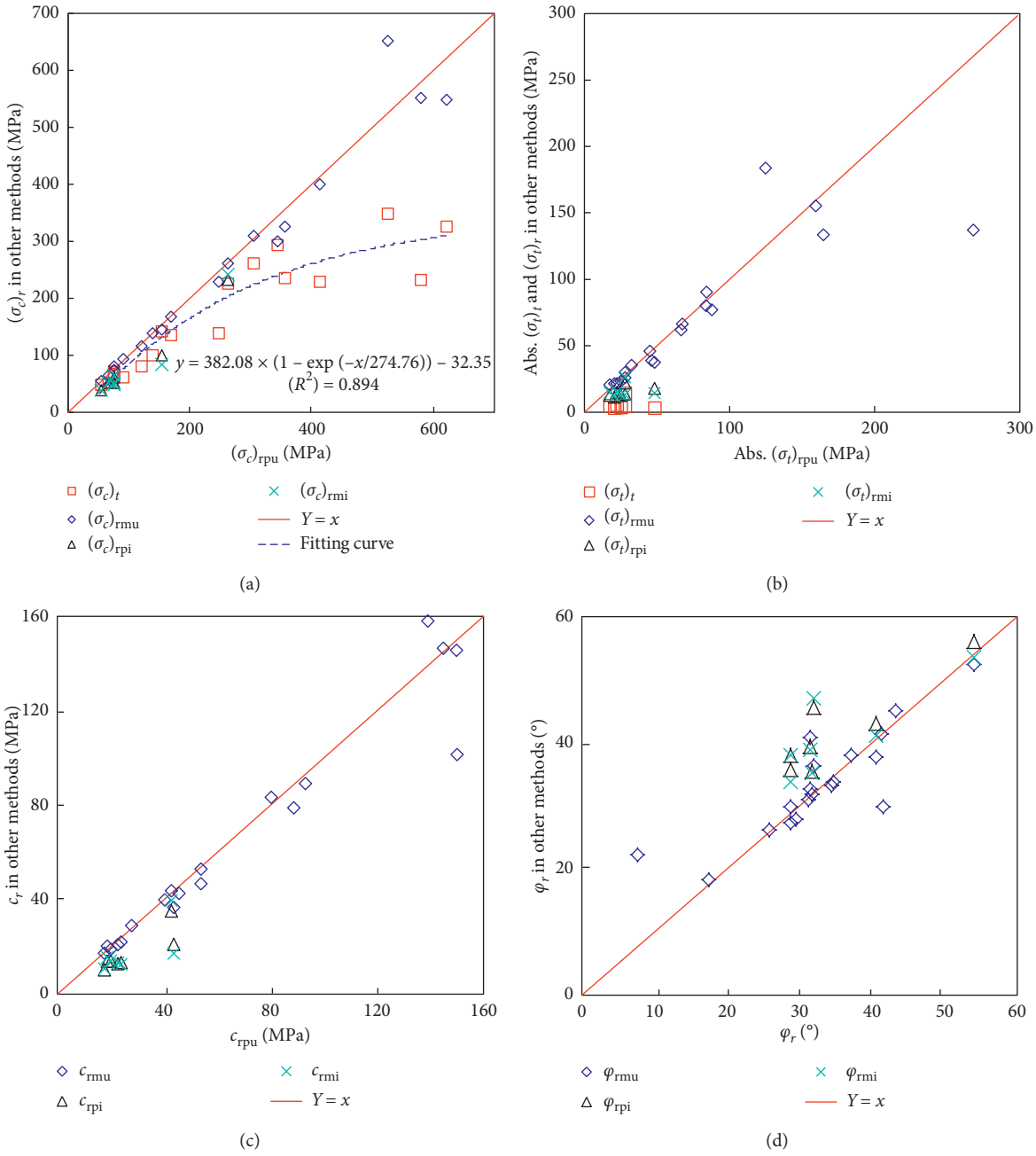

Figure 4: $(\sigma_c)_r$, $(\sigma_t)_r$, c_r, and φ_r predicted by regression of equation (1) in two stress spaces. (a) $(\sigma_c)_r$. (b) $(\sigma_t)_r$. (c) c_r. (d) φ_r.

about equal to φ_{rmu}, and it has a linear relation with φ_{rmu}. But there is some difference between them in the middle and lower parts of φ_{rmu}. When $(\sigma_t)_t$ is included in regression, φ_{rpi} and φ_{rmi} are close to each other, and they are mostly higher than the corresponding φ_{rpu} and φ_{rmu}.

All in all, whether $(\sigma_t)_t$ is included in regression or not, $(\sigma_c)_r$, $(\sigma_t)_r$, c_r, and φ_r predicted by linear equation in the principal stress space are similar to those obtained in the Mohr stress space with the method of fitting CTPAC. Consequently, the method of fitting CTPAC is completely suitable to obtain conventional triaxial failure envelopes in the Mohr stress space.

4. Regression Results of Nonlinear Strength Criterion

4.1. Typical Regression Curves of Specimen LG. In this section, CTPAC was fitted with equations (1)–(6), respectively, to obtain the conventional triaxial failure envelopes for 19 kinds of rock specimens when $(\sigma_t)_t$ is not included in regression and for 7 kinds of rock specimens when $(\sigma_t)_t$ is included in regression in the Mohr stress space.

Under the maximum normal stress σ of 139 MPa in the Mohr stress space, regression curves of specimen LG were taken as examples to analyze the regression validities of all

empirical equations as shown in Figure 5. $(\sigma_t)_t$ is not included in regression in Figure 5(a), and $(\sigma_t)_t$ is included in regression in Figure 5(b). Figure 5 shows that the regression curves are close to each other in the middle range of the tangent points, but they are divergent in the two ends, especially when the tangent points are lower. The linear regression curves (equation (1)) are below the tangent points in the middle range of the tangent points, and they are above the tangent points in two ends of the tangent points. Moreover, the parabolic regression curves (equation (2)) also have larger deflections, but they are above the tangent points in the middle of the tangent points and below the tangent points in two ends of the tangent points. Thus, R^2 of these two equations should be relatively lower. However, the other nonlinear regression curves show good regression validities, and most of them coincidently go through the tangent points.

The diverging characteristics in the lower range of the tangent points are described as follows: in Figure 5(a), when $(\sigma_t)_t$ is not included in regression, the logarithmic regression (equation (4)), hyperbolic regression (equation (5)), and exponential regression curves (equation (6)) are invariably close to tangent points and achieve a good regression result. However, the regression validities are better when $(\sigma_t)_t$ is included in regression as shown in Figure 5(b); thus the regression cohesions (c_r) and the x-intercepts of these three failure envelopes (equations (6), (8), and (10)) are more accurate. Based on the method of uniaxial tension with Mohr's circles being tangent to the envelopes, the tensile strengths predicted by regression envelopes from low to high are, respectively, as follows: parabolic equation (equation (2)), power equation (equation (3)), logarithmic equation (equation (4)), hyperbolic equation (equation (5)), exponential equation (equation (6)), and linear equation (equation (1)).

4.2. Regression Squared Correlation Coefficients. Figure 6 depicts the relationships between the squared correlation coefficients R^2 of the six equations, which are used to fit conventional triaxial failure envelopes in the Mohr stress space and maximum σ_3/σ_c, in which $(\sigma_t)_t$ is not included in regression as shown in Figure 6(a), while $(\sigma_t)_t$ is included in regression as shown in Figure 6(b).

In Figure 6, compared to nonlinear equations, R^2 of linear equation (equation (1)) are lowest on the whole and decrease with increasing maximum σ_3/σ_c. When $(\sigma_t)_t$ is not included in regression, R^2 of parabolic equation (equation (2) in Figure 6(a)) are also lower obviously and increase on the whole with increasing maximum σ_3/σ_c. The fit accuracy of other equations is all higher, and their minimums, averages, and maximums of R^2 are above 0.985, above 0.996, and close to 1.000, respectively. When $(\sigma_t)_t$ is included in regression, as for the average value, R^2 of nonlinear equations used in the Mohr stress space become higher or remain unchanged but R^2 of linear equation (equation (1)) become lower a little in Figure 6(b) compared with those in Figure 6(a). All in all, the power equation (equation (3)), the logarithmic equation (equation (4)), the hyperbolic equation (equation (5)), and the exponential equation (equation (6)) are recommended to fit conventional triaxial failure envelopes for their higher R^2.

4.3. The x-Intercepts of the Regression Curves of τ and σ in the Mohr Stress Space. In the Mohr stress space, if the x-intercept of the regression curve is positive, the y-intercept of the regression curves must be negative. In this case, regression cohesion c_r, regression uniaxial compression strength $(\sigma_c)_r$, and regression tension strength $(\sigma_t)_r$ of specimens cannot be predicted correctly by the failure envelopes. Therefore, these regression equations are not suitable for fitting the failure envelopes in the Mohr stress space if some x-intercepts of the regression curves are positive. Figure 7 shows the x-intercepts of the regression envelopes. The x-intercepts of the regression nonlinear envelopes are larger than those of the linear envelopes. No matter $(\sigma_t)_t$ is included or not included in regression, some x-intercepts of the parabolic envelope (equation (2)) and the power envelopes (equation (3)) are positive, which show that c_r, $(\sigma_c)_r$, and $(\sigma_t)_r$ may not be obtained when parabolic equation (equation (2)) and power equation (equation (3)) are used in the Mohr stress space. Thus, logarithmic equation (equation (4)), hyperbolic equation (equation (5)), and exponential equation (equation (6)) are optimal to fit the failure envelopes in the Mohr stress space. Moreover, when $(\sigma_t)_t$ is included in regression (Figure 7(b)), the x-intercepts of the logarithmic regression (equation (4)), hyperbolic regression (equation (5)), and exponential regression curves (equation (6)) are more concentrated than those with $(\sigma_t)_t$ being not included in regression. All in all, the logarithmic equation (equation (4)), the hyperbolic equation (equation (5)), and the exponential equation (6) are recommended to fit conventional triaxial failure envelopes for they have no positive x-intercepts.

4.4. c_r Predicted by the Relationship between τ and σ in the Mohr Stress Space. We know from Figure 6 that the squared correlation coefficients of logarithmic equation (equation (4)), hyperbolic equation (equation (5)), and exponential equation (equation (6)) are higher, and their failure envelopes go through nearly all tangent points in the Mohr stress space when $(\sigma_t)_t$ is included in regression; thus the cohesion c_r predicted by the above three envelopes should be closer to their true values, and the above three regression envelopes of the same set of tangent points are relatively close to each other. Besides, we know from Figure 7 that some x-intercepts of two regression envelopes of parabolic equation (equation (2)) and power equation (equation (3)) are positive, so some c_r cannot get obtained; therefore, c_r predicted by power envelopes (equation (3)) and parabolic envelopes (equation (2)) are not shown in Figure 8.

Figure 8 depicts that c_r predicted by nonlinear envelopes are all lower than those predicted by linear envelope (equation (1)). Thus, c_r predicted by linear regression envelope (equation (1)) is significantly larger and is far from the true values. In particular, c_r predicted by logarithmic (equation (4)), hyperbolic (equation (5)), and exponential

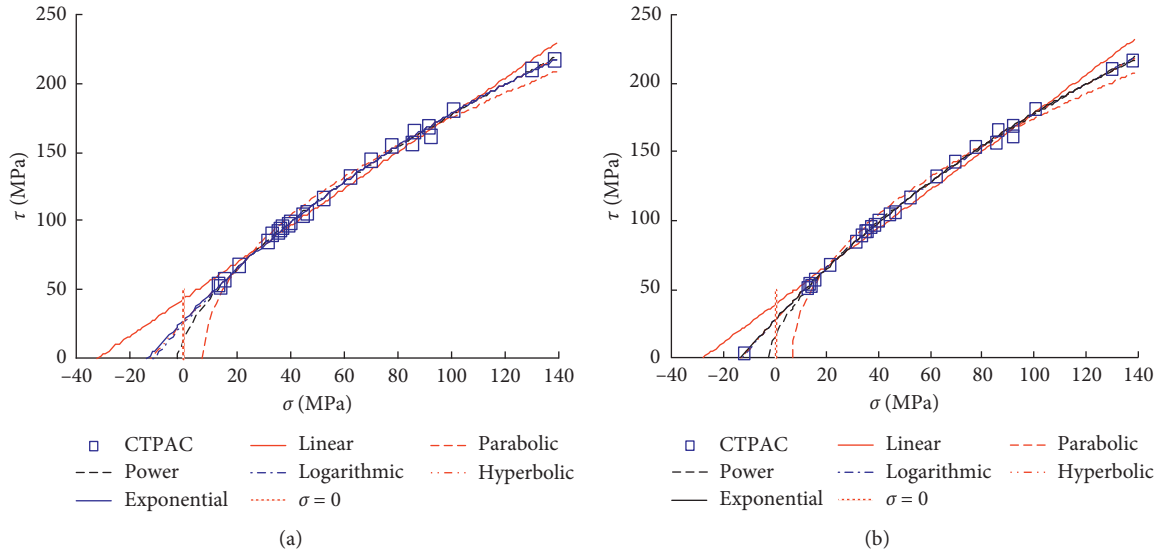

Figure 5: Typical strength envelope regression curves of specimen LG in the Mohr stress space. (a) $(\sigma_t)_t$ is not included in regression. (b) $(\sigma_t)_t$ is included in regression.

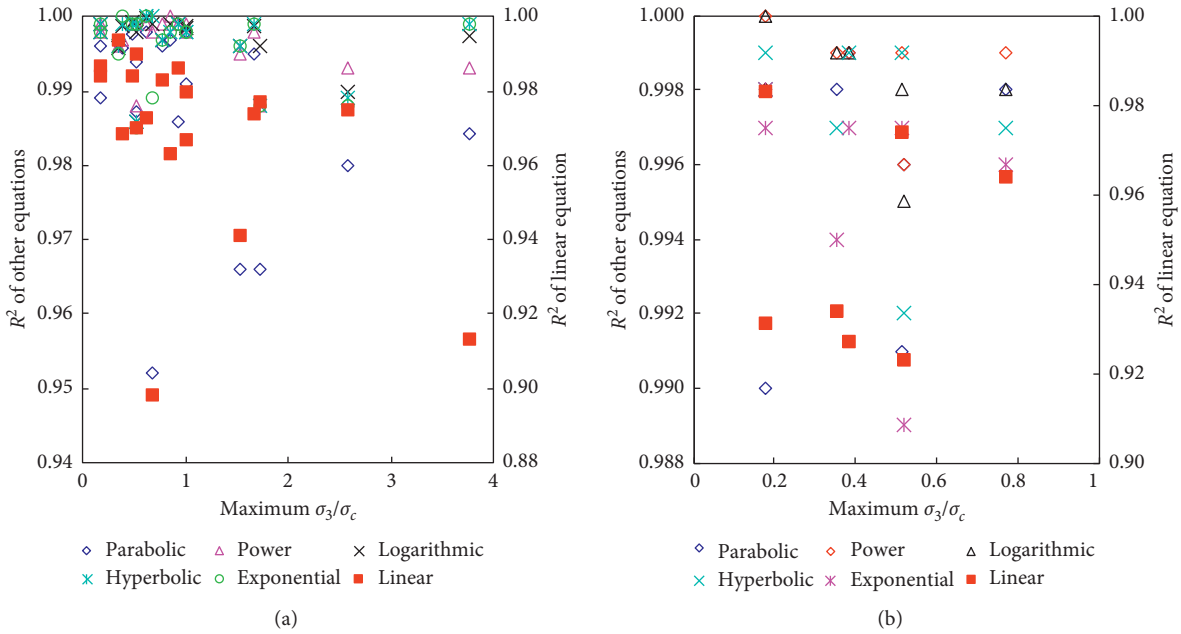

Figure 6: Regression R^2 in the Mohr stress space. (a) $(\sigma_t)_t$ was not included. (b) $(\sigma_t)_t$ was included.

(equation (6)) envelopes with $(\sigma_t)_t$ being included in regression are more focused than those predicted by the above three regression strength envelopes with $(\sigma_t)_t$ being not included in regression. Thus, using $(\sigma_t)_t$ in regression could improve the regression validities of logarithmic (equation (4)), hyperbolic (equation (5)), and exponential equations (equation (6)). $(\sigma_t)_t$ are advised to be included in fitting nonlinear failure envelopes to get more accurate conventional triaxial strength parameters. The logarithmic equation (equation (4)), the hyperbolic equation (equation (5)), and the exponential equation (equation (6)) are all recommended to fit conventional triaxial failure envelopes for they have relatively close c_r.

5. Friction and Cohesion Bearing Characteristics of a Rock Specimen

5.1. Negative Friction Bearing Capacity. In order to explain the existence of negative friction bearing capacity, the stress diagram of potential failure plane of a specimen under triaxial compression is shown in Figure 9. When the axial pressure σ_1 and the confining pressure σ_3 are positive (Figure 9(a)), their components in the potential failure plane are the normal compressive stress component σ_{3n} in the downward vertical direction of the potential failure plane and the shear stress component $\sigma_{3\tau}$ in the upward parallel direction of potential failure plane. The components of axial

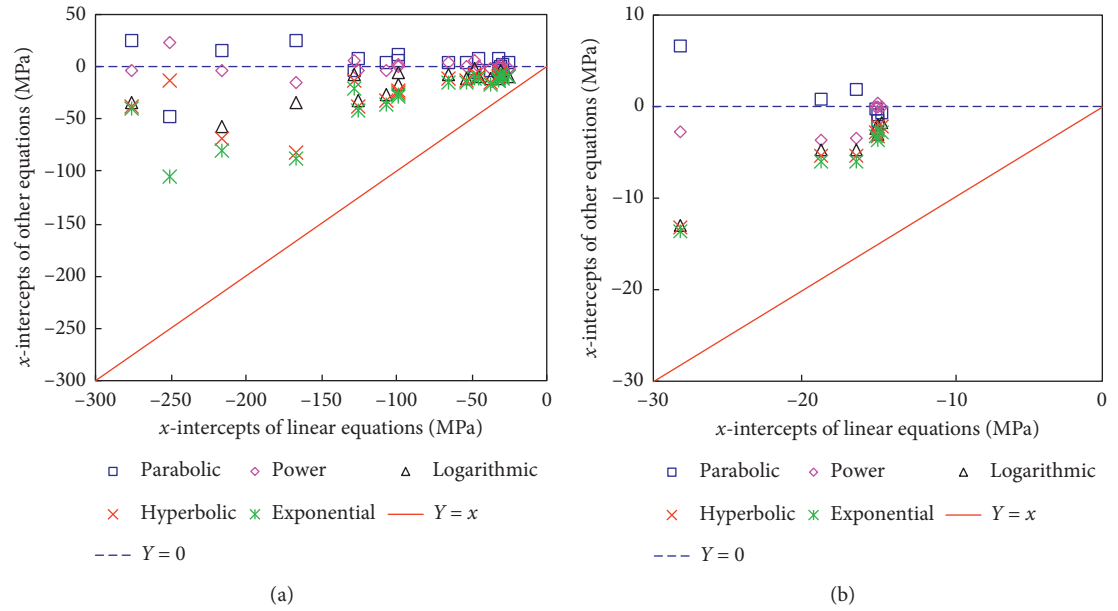

FIGURE 7: The x-intercepts of the regression strength envelopes. (a) $(\sigma_t)_t$ is not included in regression. (b) $(\sigma_t)_t$ is included in regression.

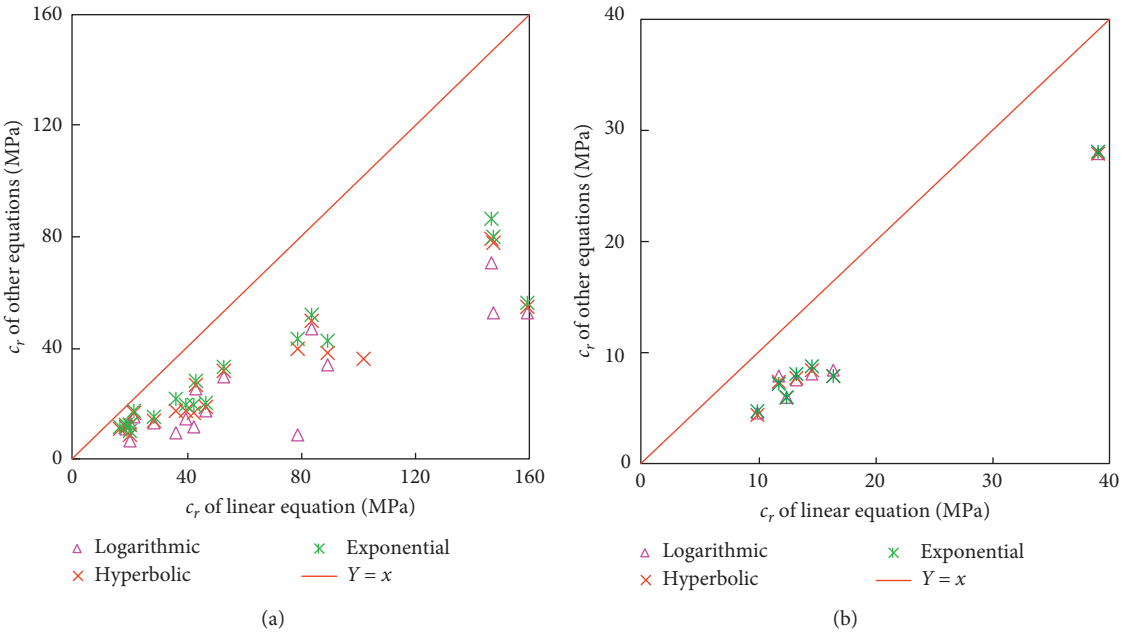

FIGURE 8: c_r predicted by regression relationship between τ and σ in the Mohr stress space. (a) $(\sigma_t)_t$ is not included in regression. (b) $(\sigma_t)_t$ is included in regression.

pressure σ_1 in the potential failure plane are the normal compressive stress component σ_{1n} in the downward vertical direction of the potential failure plane and the shear stress component $\sigma_{1\tau}$ in the downward parallel direction of the potential failure plane. Thus, the composition of the total bearing capacity Q can be expressed as

$$Q = Q_s = Q_f + Q_c, \tag{8}$$

$$Q_s = \iint_{\Sigma} (\sigma_{1\tau} - \sigma_{3\tau})\, \mathrm{d}S, \tag{9}$$

$$Q_f = k_1 \iint_{\Sigma} (\sigma_{1n} + \sigma_{3n})\, \mathrm{d}S, \tag{10}$$

$$Q_c = \iint_{\Sigma} c\, \mathrm{d}S, \tag{11}$$

where S is the failure fracture surface area, both the friction bearing capacity Q_f and cohesion bearing capacity Q_c are positive, so that the total bearing capacity Q is larger than the cohesion bearing capacity Q_c, and the friction bearing

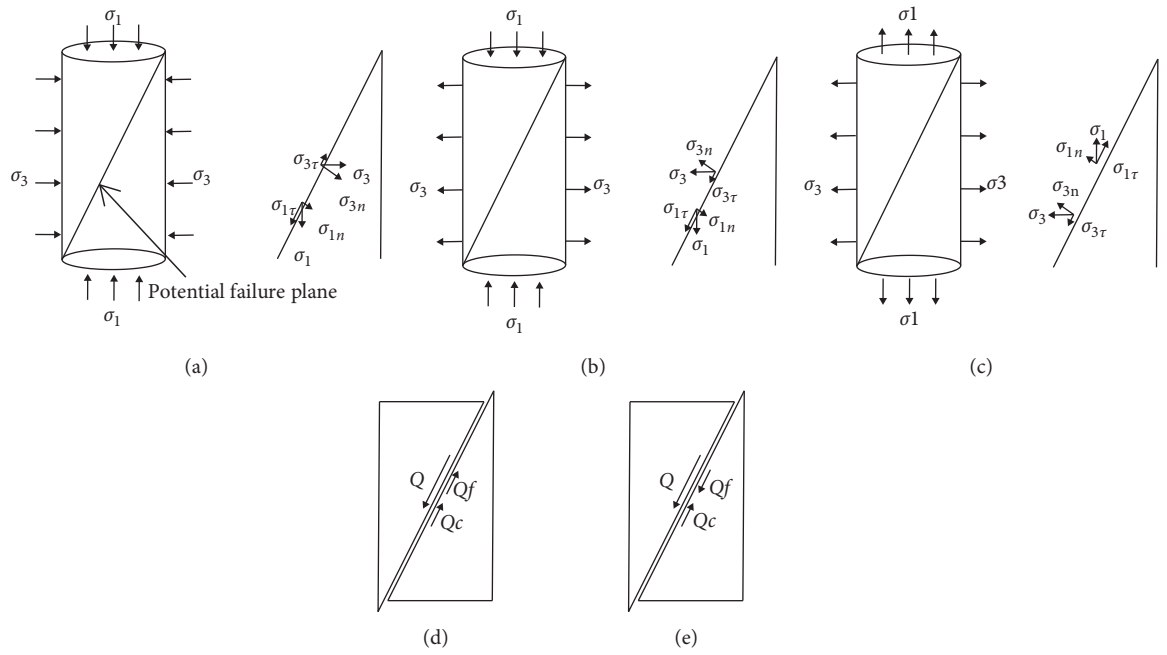

Figure 9: Stress diagram of potential failure plane of a specimen under triaxial compression.

capacity $Q_f > 0$ and can be named as a positive one (Figure 9(d)). Besides, the directions of the above two shear stress components are contrary; therefore, when the specimen fails and slides down along the fracture surface, the shear force produced by the confining pressure σ_3 in the opposite direction is not conducive to the failure of the potential failure plane and will increase the axial pressure σ_1 at failure.

When the axial pressure σ_1 is positive and the confining pressure σ_3 is negative (Figure 9(b)), the component directions of the confining pressure σ_3 in the potential failure plane will be opposite to the condition that it is positive. That is to say, when the axial pressure $\sigma_1 > 0$ and the confining tensile stress $\sigma_3 < 0$, these two shear stress components are both in the downward parallel direction of potential failure plane; therefore, when the specimen fails and slides down along the fracture surface, the shear force produced by the confining pressure σ_3 in the same direction is conducive to the failure of the potential failure plane and will decrease the axial pressure σ_1 at failure. Under these circumstances, the cohesion bearing capacity Q_c is a positive constant, while the friction bearing capacity Q_f may be positive or negative according to the value of $\sigma_{1n} + \sigma_{3n}$, so that the total bearing capacity Q may be higher or lower than the cohesion bearing capacity Q_c, and the friction bearing capacity Q_f can be named as a negative one when $Q_f < 0$ (Figure 9(f)).

When the confining pressure σ_3 and the axial pressure σ_1 are both negative (Figure 9(c)), the cohesion bearing capacity Q_c is still a positive constant, while the friction bearing capacity Q_f is negative according to the value of $\sigma_{1n} + \sigma_{3n}$, so that the total bearing capacity Q is lower than the cohesion bearing capacity Q_c, and the friction bearing capacity Q_f is a negative one (Figure 9(f)).

The above analysis expresses the possibility of the existence of negative friction bearing capacity Q_f; in order to understand the above analysis more clearly in the Mohr stress space as shown in Figure 10, a further explanation is made here.

The tangent point P of circle O_1 and linear strength envelope is on the vertical axis, and the value of P at the vertical coordinate is the cohesion c of a rock. When the ultimate stress circle is on the right side of circle O_1, the friction bearing capacity Q_f is positive, and the total bearing capacity is higher than the cohesion bearing capacity Q_c; when the ultimate stress circle is on the left side of circle O_1, the friction bearing capacity Q_f is negative, and the total bearing capacity Q is lower than the cohesion bearing capacity Q_c.

5.2. Friction and Cohesion Bearing Characteristics of Rock in Linear Strength Criterion. Friction and cohesion will not work for one point at the same time in a rock specimen [8]. That is to say, every point on the potential failure plane cannot provide friction and cohesion at the same time. When the point is not damaged, it provides bearing capacity with cohesion; when the point is damaged, it provides bearing capacity with friction. Evolution schematic diagram of rock bearing capacity composition is shown in Figure 11, in which total bearing capacity Q is the sum of the cohesion bearing capacity Q_f and the friction bearing capacity Q_c. As shown in Figure 11(a), when a linear equation is used in regression, the friction coefficient of rock $k = \tan\varphi$ is a constant, and the cohesion bearing capacity Q_c is also a constant, but the total bearing capacity Q and friction bearing capacity Q_f increase linearly as the normal stress σ increases. The contribution proportion of cohesion bearing capacity Q_c to increment of total bearing capacity ΔQ is 0, while the increment of friction bearing capacity ΔQ_f is equal to the increment of total bearing capacity ΔQ with the

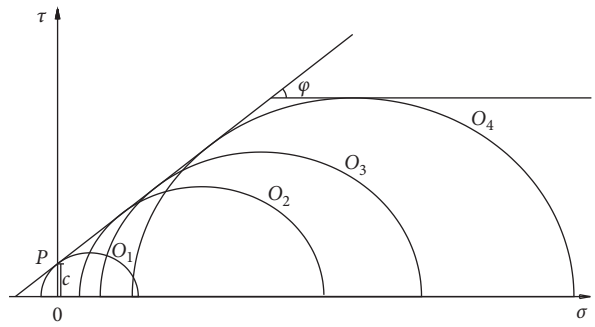

Figure 10: Relationship between rock bearing capacity composition and ultimate stress circles.

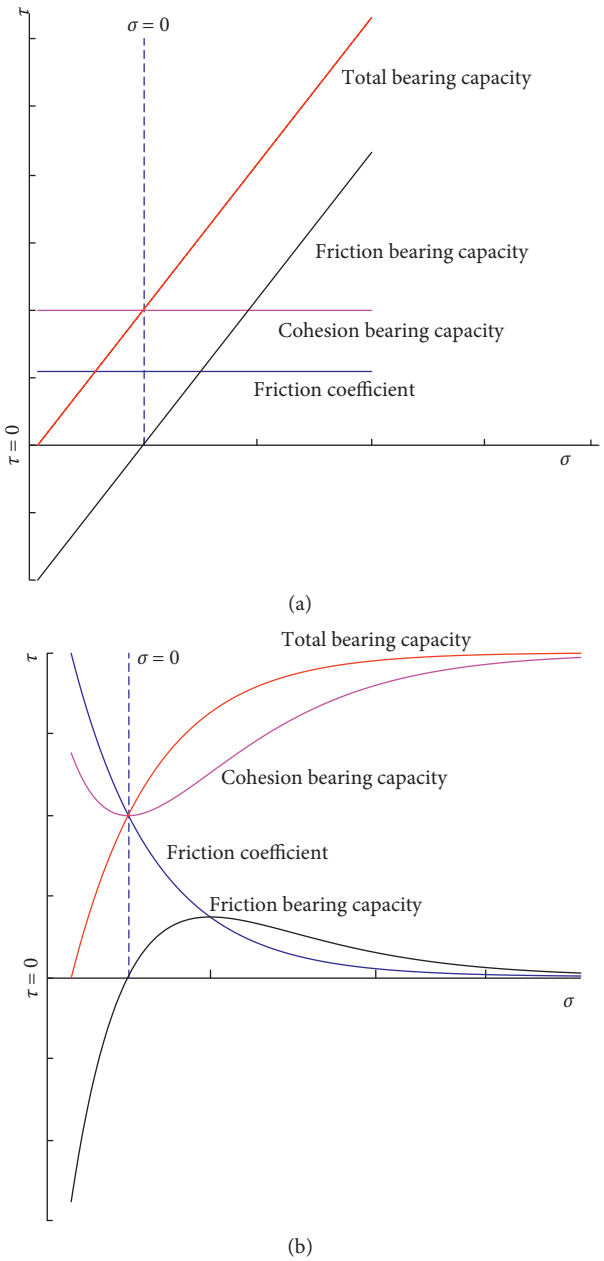

Figure 11: Evolution schematic diagram of rock bearing capacity composition. (a) Linear strength envelope. (b) Nonlinear strength envelope.

normal stress increasing, and the ratio of friction bearing capacity Q_f to total bearing capacity Q approaches 100% finally. When the normal stress σ is less than 0, there is a negative friction bearing capacity Q_f that counteracts a same value of cohesion bearing capacity Q_c, thus reducing the total bearing capacity Q.

5.3. Friction and Cohesion Bearing Characteristics of Rock in Nonlinear Strength Criterion. When nonlinear equations are used in regression, friction coefficients are all reducing variables that decrease with the increase of normal stress. It means that the frictional coefficient is larger when the normal stress is lower, and it is lower when the normal stress is larger. So, the contribution proportion of friction bearing capacity ΔQ_f to the increment of total bearing capacity ΔQ gradually reduces and even disappears in the end with increasing normal stress. Barton [20] divided shear strength envelope of rock joint under different normal stress into two parts by a critical normal stress. When the normal stress is lower than the critical normal stress, the friction coefficient is large as it is the tangent value of two angles: a friction angle and a climbing angle; when the normal stress exceeds the critical value, the frictional coefficient is small as it is only the tangent value of the friction angle. There is a similar viewpoint here, but the friction coefficient decreases gradually with normal stress increasing. However, the difference is that the friction coefficient in nonlinear strength criteria is always a nonlinear curve but is not only two constants as in Barton's method [17].

As normal stress increases, total bearing capacity Q increases with a reducing increasing rate as shown in Figure 11(b), the friction coefficient k decreases gradually, the cohesion bearing capacity Q_c decreases firstly and then increases before and after the normal stress is 0 MPa, and the friction bearing capacity Q_f increases firstly and then decreases. It needs to be explained that the cohesion bearing capacity Q_c of the rock specimen under each normal stress is the intercept of the tangent line of each corresponding point on the total bearing capacity curve on the longitudinal axis, the friction coefficient k of the rock specimen under each normal stress is the tangent slope value of each corresponding point on the total bearing capacity curve, and the friction bearing capacity Q_f of the rock specimen under each normal stress is the product of the normal stress σ and its corresponding friction coefficient k.

According to the above assumption, when the normal stress is less than 0, there is a negative friction bearing capacity Q_f and a larger positive cohesion bearing capacity Q_c; when the normal stress is 0, friction bearing capacity Q_f is 0 and the cohesion bearing capacity Q_c reaches its lowest value; when the normal stress is larger than 0, as the normal stress increases, the friction bearing capacity Q_f increases firstly and then decreases to approach 0 gradually, while the cohesion bearing capacity Q_c increases to approach the total bearing capacity Q gradually. When the normal stress rises to infinity, the frictional angle will tend to be zero and the increment of friction bearing capacity ΔQ_f also tends to be zero with increasing normal stress, and the friction bearing

capacity Q_c is close to the total bearing capacity Q under this condition; thus the total bearing capacity Q and its increment ΔQ will be provided by only the cohesion bearing capacity Q_c and its increment ΔQ_c. Therefore, if the increment of cohesion bearing capacity ΔQ_c has a limit, the total bearing capacity Q also has a limit; otherwise, the total bearing capacity Q of rock will increase with the increment of cohesion bearing capacity ΔQ_c in a same quantity. If the former is in existence, the hyperbolic equation and the exponential equation are more suitable for fitting triaxial compression strengths in a higher maximum confining pressure range in the Mohr stress space.

If used to evaluate the strength characteristics of rock in high-stress state at deep or extra deep depts, the applicability of the empirical equations obtained from the test data with a lower maximum confining pressure needs a further study. Only by determining the strength characteristics of rock in the high confining pressure range can a more reasonable rock strength criterion be determined in the lower confining pressure range, and the rock strength criterion can be used without confining pressure range restriction. If a reasonable strength criterion and its parameters are determined only based on the test data in a lower confining pressure range, the applicability of the criterion and parameters under high confining pressure will be more questioned. Therefore, the next step should be to improve the rock mechanical equipment and test methods, obtain the strength test data of higher confining pressure range, determine the characteristics of rock bearing capacity limit, and then determine a more reasonable rock strength criterion.

6. Conclusions

The following conclusions were reached in this research study:

(1) Whether $(\sigma_t)_t$ is included or not included in regression, $(\sigma_c)_r$, $(\sigma_t)_r$, c_r, and φ_r predicted by linear equation in the principal stress space are similar to those obtained in the Mohr stress space with the method of fitting CTPAC, and thus the method of fitting CTPAC is completely suitable to obtain conventional triaxial failure envelopes in the Mohr stress space.

(2) The squared correlation coefficients of linear equation are generally lower than those of nonlinear equations and would further reduce when $(\sigma_t)_t$ is included in regression. $(\sigma_c)_t$ are lower than all the corresponding predicted values and have an exponential relation with $(\sigma_c)_{\mathrm{rpu}}$ when $(\sigma_t)_t$ is not included in regression. $(\sigma_c)_r$ and Abs. $(\sigma_t)_r$ are more closer to their test values, respectively, when $(\sigma_t)_t$ is included in regression.

(3) In the Mohr stress space, logarithmic equation, hyperbolic equation, and exponential equation are recommended to fit conventional triaxial failure envelopes because some x-intercepts of the regression curve of power equation and parabolic equation are positive. Using $(\sigma_t)_t$ in regression can further improve the regression validities.

(4) According to the assumption that the cohesion is constant, the negative friction bearing capacity exists when the ultimate stress circle is on the left side of the critical ultimate stress circle whose tangent point and strength envelope are on the longitudinal axis. Through the analysis of the evolution process of the nonlinear strength envelope, it is considered that when the normal stress is infinite, the total bearing capacity of a rock is about equal to the cohesive bearing capacity, while the friction no longer provides the bearing capacity. It is concluded that the hyperbolic equation and the exponential equation are more suitable to fit triaxial compression strength under higher maximum confining pressures for they have limit values.

Data Availability

The research data used to support the findings of this study are included within the article. Request for more details should be made to the corresponding author.

Conflicts of Interest

The authors declare no conflicts of interest.

Acknowledgments

The authors acknowledge the financial support of the National Natural Science Foundation of China (Grant no. 51904092), the Key Scientific Research Project of Higher Education Institutions in Henan Province (Grant no. 20B580002), and the Fundamental Research Funds for the Universities of Henan Province (Grant no. NSFRF180336).

References

[1] B. Yazdani Bejarbaneh, D. Jahed Armaghani, and M. F. Mohd Amin, "Strength characterisation of shale using mohr-coulomb and hoek-brown criteria," *Measurement*, vol. 63, pp. 269–281, 2015.

[2] G. Tsiambaos and N. Sabatakakis, "Considerations on strength of intact sedimentary rocks," *Engineering Geology*, vol. 72, no. 3-4, pp. 261–273, 2004.

[3] J. Zhao, "Applicability of mohr-coulomb and hoek-brown strength criteria to the dynamic strength of brittle rock," *International Journal of Rock Mechanics and Mining Sciences*, vol. 37, no. 7, pp. 1115–1121, 2000.

[4] J. V. Stafford, E. Audsley, and J. R. Sharp, "The determination of best fit linear failure envelopes to mohr circles," *Journal of Agricultural Engineering Research*, vol. 33, no. 1, pp. 33–38, 1986.

[5] X. H. Wang, "Regression solution for general stress intensity of the tri-axis shearing," *Journal of Earth Science and Environment*, vol. 26, pp. 52–54, 2004.

[6] T. Yang, C. Xu, and B. X. Wang, "The cohesive strength and friction angle in rock-soil triaxial tests," *China Mining Magazine*, vol. 16, pp. 104–107, 2007.

[7] M. Q. You, "Study of deformation and failure of rock based on properties of cohesion and friction," *Journal of Geomechanics*, vol. 11, pp. 286–292, 2005.
[8] M. You, "Mechanical characteristics of the exponential strength criterion under conventional triaxial stresses," *International Journal of Rock Mechanics and Mining Sciences*, vol. 47, no. 2, pp. 195–204, 2010.
[9] M. Sari, "An improved method of fitting experimental data to the hoek-brown failure criterion," *Engineering Geology*, vol. 127, pp. 27–35, 2012.
[10] H. Bineshian, A. Ghazvinian, and Z. Bineshian, "Comprehensive compressive-tensile strength criterion for intact rock," *Journal of Rock Mechanics and Geotechnical Engineering*, vol. 4, no. 2, pp. 140–148, 2012.
[11] M. You, "Comparison of the accuracy of some conventional triaxial strength criteria for intact rock," *International Journal of Rock Mechanics and Mining Sciences*, vol. 48, no. 5, pp. 852–863, 2011.
[12] X. Si, F. Gong, X. Li, and S. Luo, "Dynamic mohr-coulomb and hoek-brown strength criteria of sandstone at high strain rates," *International Journal of Rock Mechanics and Mining Sciences*, vol. 115, pp. 48–59, 2019.
[13] X. F. Wang, F. Q. Gong, X. B. Li et al., "Rock dynamic mohr-coulomb and hoek-brown criteria based on strain rate effect," *The Chinese Journal of Nonferrous Metals*, vol. 26, pp. 1763–1773, 2016.
[14] E. Catrin, *Rock Mass Strength: A Review*, Lule Tekniska Universitet, Luleå, Sweden, 2003.
[15] Y. S. Fu, *Fitting and Evaluation of the Conventional Triaxial Strength Criteria with Test Data*, M.S. thesis, Henan Polytechnic University, Jiaozuo City, China, 2012.
[16] B. J. Carter, E. J. Scott Duncan, and E. Z. Lajtai, "Fitting strength criteria to intact rock," *Geotechnical and Geological Engineering*, vol. 9, no. 1, pp. 73–81, 1991.
[17] K. Mogi, *Experimental Rock Mechanics*, Taylor & Francis, London, UK, 2007.
[18] M. Q. You, "Three independent parameters to describe conventional triaxial compressive strength of intact rocks," *Journal of Rock Mechanics and Geotechnical Engineering*, vol. 4, pp. 350–356, 2010.
[19] L. Zhang, S. Z. Wang, and L. Q. Shi, "The strength characteristics of six types of rocks under high minor principal stress," *Chinese Journal of Rock Mechanics and Engineering*, vol. 4, pp. 10–19, 1985.
[20] N. Barton, "Shear strength criteria for rock, rock joints, rockfill and rock masses: problems and some solutions," *Journal of Rock Mechanics and Geotechnical Engineering*, vol. 5, no. 4, pp. 249–261, 2013.